Roi Segmentation on Lung Ct Images in Noisy Environment

P.Sahithi, PG Scholor, Dept. of ECE, Narayana Engg. College, Nellore – 524004,
KS. Sagar Reddy, Sr. Asst. Professor, Dept. of ECE, Narayana Engg. College, Nellore – 524004,
P.Sindhooi, Asst. Professor, Dept. of ECE, Narayana Engg. College, Nellore – 524004,

ABSTRACT:
Various medical imaging available are MRI, CT, US and DICOM in which the DICOM (Digital Imaging and Communications in Medicine) standard is the backbone of modern image display. Automated Computer Aided Diagnosing (CAD) system detects lung cancer. The use of CAD systems improves the sensitivity diagnostic radiology research. Several approaches are used to lung CAD combine geometric and intensity models to enhance local anatomical structure (e.g. spherical objects). Two difficulties those are primarily associated with the detection of nodules include the detection of nodules that are adjacent to vessels or the chest wall when they have very similar intensity; and the detection of nodules that are non-spherical in shape. In such cases, intensity thresholding or model based methods might fail to identify those nodules. In this paper Region Of Interest (ROI) segmentation of DICOM lung image is performed in the noisy environment such as Gaussian, Poisson, speckle, salt and pepper noise. The ROI lung area nodules from the major lung portion are achieved using different edge detection operators such as Average, Gaussian, Laplacian, Sobel, Prewitt, Laplacian, LoG and Unsharp filters with and without noise. The results are helpful to study and analyze the influence of noises such as Gaussian, Poisson, Salt & pepper and speckle on the DICOM images.

Keywords: Lung CT Images, DICOM, ROI, Noise and filters

1. INTRODUCTION:

LUNG Cancer is one of the most serious health problems in the world field. The mortality rate of lung cancer is the highest among all other types of cancer. Lung cancer is one of the most serious cancers in the world, with the smallest survival rate after the diagnosis, with a gradual increase in the number of deaths every year. Survival from lung cancer is directly related to its growth at its detection time. The earlier the detection is, the higher the chances of successful treatment are. An estimated 85% of lung Cancer cases in males and 75% in females are caused by cigarette smoking. The overall survival rate for all types of cancer is 63%. Although surgery, radiation therapy, and chemotherapy have been used in the treatment of lung cancer, the five year survival rate for all stages combined is only 14%. This has not changed in the past three decades. The purpose of this work is to develop a CAD system for early detection of lung cancer based on an automatic diagnosis of the lung regions included in chest DICOM images. The difficulties for detecting lung nodules in radiographs are below:

- Nodule sizes are varying widely: Commonly a nodule diameter can take any value between a few millimeters up to several centimeters.
- Nodules exhibit a large variation in density – and Hence visibility on a radiograph some nodules are only slightly denser than the surrounding lung tissue, while the densest ones are calcified.
- Nodule that are non spherical in shape.
- As nodules can appear anywhere in the lung field, detection of nodules that are adjacent to vessels or the chest walls when they have similar intensity.
- Poor quality of the image.

However, a major problem in the screening for lung cancer by the radiologist with DICOM is the fact that the objects to recognize in the image slices, such as nodules, blood vessels and bronchi, often have similar characteristics in terms of density, shape and size. To help solve this problem a computer-aided diagnosis (CAD) system is developed for detection of pulmonary nodules on DICOM images. Image segmentation is an important process in most

medical image analysis tasks. An image segmentation logarithm decomposes an image into regions having visual similarity and strong statistical correlation. Extraction and classification of cervical cells is an important process that has many applications in medical imaging. A good segmentation algorithm will benefit radiologists and patients as they provide important information for 3-D visualization, surgical planning and early disease detection.

Mathematical morphology (MM), a set theoretic, shape oriented approach treats the image as a set and the kernel of operation commonly known as structuring element (SE) as another set. Different standard morphological operations like dilation, erosion, opening, closing are basically set theoretic operations between these two sets. The shape and the size of the SE play an important role in detecting and extracting features of shape and size of the objects in the image, its different sizes can be accounted by the 'scale' attribute of the structuring element. Thus morphological operations with such scalable SEs can be used in multiscale image segmentation. The watershed transform coming from the field of mathematical morphology plays an important role in medical image segmentation.

A fast and flexible algorithm for computing watersheds in digital grayscale images was introduced by Luc Vincent and Pierre Soille. The watershed transform possesses number of advantages: it is a simple intuitive method, it is fast and can be parallelized and it produces a complete division of the image in separated regions even if the contrast is poor, thus avoiding the need for any kind of contours joining.

The nodule detection provides a rough surface to the cervical cancer image for which watershed segmentation has better features for analysis when compared to the simple edge analysis, since the morphological watershed segmentation embodies the basic principal concepts such as detection of discontinuity, thresholding and region processing apart from producing more stable segmentation results, including the continuous segmentation boundaries. Watershed technique is one of the classical techniques in the field of topography providing a simple framework for incorporating the knowledge based constraints in the segmentation process. When combined with other morphological tools, the watershed transformation becomes a basis for extremely powerful segmentation procedures.

2. NOISE MODELING AND IMAGE FILTERING:

2.1 BRIEF DESCRIPTION:

Noise represents unwanted information which deteriorates image quality. Noise is defined as a process (*n*) which affects the acquired image (*f*) and is not part of the scene (initial signal – *s*). Using the additive noise model, this process can be written as:

$$f(i, j) = s(i, j) + n(i, j) \quad (1)$$

Digital image noise may come from various sources. The acquisition process for digital images converts optical signals into electrical signals and then into digital signals and is one processes by which the noise is introduced in digital images. Each step in the acquisition process may introduce random changes into the values of pixels in the image. These changes are called noise. .

2.2 TYPES OF NOISE IN IMAGES:

Noise can generally be grouped into two classes:

- Image data Independent noise.
- Noise which is dependent on the image data.

Image independent noise can often be described by an additive noise model, where the recorded image f(i, j) is the sum of the true image s(i, j) and the noise n(i, j):

$$f(i, j) = s(i, j) + n(i, j) \quad (2)$$

The noise n(i, j) is often zero-mean and described by its variance σ_n^2. The impact of the noise on the image is often described by the signal to noise ratio (SNR), which is given by

$$SNR = \frac{\sigma_s}{\sigma_n} = \sqrt{\frac{\sigma_f^2}{\sigma_n^2} - 1} \quad (3)$$

Where, σ_n^2 and σ_f^2 are the variances of the true image and the recorded image, respectively. In many cases, additive noise is evenly distributed over the frequency domain (i.e. white noise), whereas an image contains mostly low frequency information. Hence, the noise is dominant for high frequencies and its effects can be reduced using some kind of low pass filter. This can be done either with a frequency filter or with a spatial filter. (Often a spatial filter is preferable, as it is computationally less expensive than a frequency filter.) In the second case of data-dependent noise (e.g. arising when monochromatic radiation is scattered from a surface whose roughness is of the order of a wavelength, causing wave interference which results in image speckle), it is possible to model noise with a multiplicative, or non-linear, model. These models are mathematically more complicated; hence, if possible, the noise is assumed to be data independent.

2.3 GAUSSIAN NOISE:

This most common type of noise results from the contributions of many independent signals. This is a consequence of the central limit theorem which states that the sum of many random variables with various PDFs results in a signal with a Gaussian PDF. For example, the reading noise from a CCD detector is generated by the thermal fluctuations in many interconnected electronics components and, thus, has a Gaussian PDF.

Gaussian noise has a normal probability density function:

$$PDF_{Gaussian} = \frac{1}{2\pi\sigma} e^{-\frac{(g-\mu)^2}{2\sigma^2}} \quad (4)$$

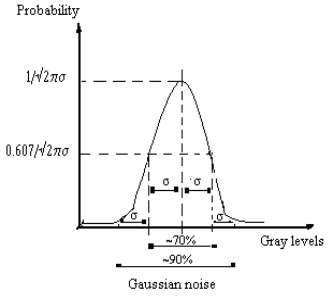

Figure 1: Probability density function for the Gaussian noise

Where:

g = gray level;
μ= mean;
σ= standard deviation;

Approximately 70% of the values are contained between $\mu \pm \sigma$and 90% of the values are contained between $\mu \pm 2\sigma$. Although, theoretically speaking, the PDF is non-zero everywhere between $-\infty$ and $+\infty$, it is customary to consider the function 0 beyond $\mu \pm 3\sigma$.

Gaussian noise is useful for modeling natural processes which introduce noise (e.g.noise caused by the discrete nature of radiation and the conversion of the optical signal into an electrical one – detector/shot noise, the electrical noise during acquisition – sensor electrical

signal amplification, etc.).

2.4 POISSON NOISE:

The parameter λ is not only the mean number of occurrences (k), but also its variance $\sigma_k^2 = \langle k^2 \rangle - \langle k \rangle^2$. Thus, the number of observed occurrences fluctuates about its mean λ with a standard deviation $\sigma_s = \sqrt{\lambda}$. These fluctuations are denoted as Poisson noise or (particularly in electronics) as shot noise.

The correlation of the mean and standard deviation in counting independent, discrete occurrences is useful scientifically. By monitoring how the fluctuations vary with the mean signal, one can estimate the contribution of a single occurrence, even if that contribution is too small to be detected directly. For example, the charge e on an electron can be estimated by correlating the magnitude of an electric current with its shot noise. If N electrons pass a point in a given time t on the average, the mean current is $I = \frac{eN}{t}$ since the current fluctuations should be of the order $\sigma_I = \frac{e\sqrt{N}}{t}$ (i.e. the standard deviation of the Poisson process), the charge e can be estimated from the ratio $\frac{\sigma_I^2}{I}$. An everyday example is the graininess that appears as photographs are enlarged; the graininess is due to Poisson fluctuations in the number of reduced silver grains, not to the individual grains themselves. By correlating the graininess with the degree of enlargement, one can estimate the contribution of an individual grain (which is otherwise too small to be seen unaided). Many other molecular applications of Poisson noise have been developed, e.g., estimating the number density of receptor molecules in a cell membrane.

2.5 SALT & PEPPER NOISE:

Another common form of noise is data drop-out noise (commonly referred to as intensity spikes, salt and pepper noise). In the salt & pepper noise model only two possible values are possible, a and b, and the probability of obtaining each of them is less than 0.1 (otherwise, the noise would vastly dominate the image). For an 8 bit/pixel image, the typical intensity value for pepper noise is close to 0 and for salt noise is close to 255.

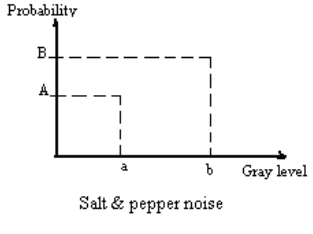

Figure 2: Probability density functions for the salt & pepper noise model.

$$PDF\ Salt\ \&\ Pepper \begin{cases} A & for\ g = a \\ B & for\ g = b \end{cases} \quad (5)$$

2.6 MULTIPLICATIVE OR SPECKLE NOISE:

Multiplicative noise, or speckle noise, is a signal dependent form of noise whose magnitude is related to the value of the original pixel. Equation (6) describes one simple form it can take, but a more complex function of the original pixel value is also possible.

$$f(i, j) = s(i, j) + n(i, j) * s(i, j) \quad (6)$$

Speckle noise is a random, deterministic, interference pattern in an image formed with coherent radiation of a medium containing many sub-resolution scatterers. The texture of the observed speckle pattern does not correspond to underlying structure. The local brightness of the speckle pattern, however, does reflect the local echogenicity of the underlying scatterers. Speckle is present in both RF data and envelope-detected data.

2.7 NOISE REDUCTION:

Digital images are prone to a variety of types of noise. There are several ways that noise can be introduced into an image, depending on how the image is created. For example: If the image is scanned from a photograph made on film, the film grain is a source of noise. Noise can also be the result of damage to the film, or be introduced by the scanner itself. If the image is acquired directly in a digital format, the mechanism for gathering the data (such as a CCD detector) can introduce noise. Electronic transmission of image data can introduce noise. Image noise elimination (reduction) is the process of removing noise from the image. Noise reduction techniques are conceptually very similar regardless of the signal being processed, however a priori knowledge of the characteristics of an expected signal can mean the implementations of these techniques vary greatly depending on the type of signal. In practice a lot of methods are used to eliminate the noise from the image and a lot of filters are used. Table (1) show a summary of some filters which are used to eliminate the noise and the results of using these filters was compared with the proposed methodology in this work.

Table 1: Standard Filters

Value	Description
Averaging	Averaging filter
Gaussian	Gaussian low pass filter
Laplacian	Filter approximating the two-dimensional laplacian operator
Sobel	Sobel horizontal edge-emphasizing filter
Prewitt	Prewitt horizontal edge-emphasizing filter
LoG	Laplacian of Gaussian filter
Unsharp	Unsharp contrast enhancement filter

3. CORRELATION COEFFICIENT, PSNR AND MAE:

3.1 CROSS CORRELATION:

Cross correlation is a standard method of estimating the degree to which two series are correlated. Consider two series x(i) and y(i) where i=0,1,2...N-1. The cross correlation r at delay d is defined as

$$\sigma_s = \frac{\sum_i [(x(i) - mx) * (y(i-d)) - my]}{\sqrt{\sum_i (x(i) - mx)^2} \sqrt{\sum_i (y(i-d) - my)^2}} \quad (7)$$

Where mx and my are the means of the corresponding series. If the above is computed for all delays d=0,1,2,...N-1 then it results in a cross correlation series of twice the length as the original series.

$$r_d = \frac{\sum_i [(x(i) - mx) * (y(i-d)) - my]}{\sqrt{\sum_i (x(i) - mx)^2} \sqrt{\sum_i (y(i-d) - my)^2}} \quad (8)$$

There is the issue of what to do when the index into the series is less than 0 or greater than or equal to the number of points. The most common approaches are to either ignore these points or assuming the series x and y are zero for i < 0 and i ≥ N. In many signal processing applications the series is assumed to be circular in which case the out of range indexes are "wrapped" back within range, i.e.: x(-1) = x(N-1), x(N+5) = x(5) etc

The range of delays d and thus the length of the cross correlation series can be less than N, for example the aim may be to test correlation at short delays only. The denominator in the expression above serves to normalize the correlation coefficients such that -1 ≤ r(d) ≤ 1, the bounds indicating maximum correlation and 0 indicating no correlation. A high negative correlation indicates a high correlation but of the inverse of one of the series. As a simple example, consider the two rectangular pulses shown below, the correlation series is shown in thick line.

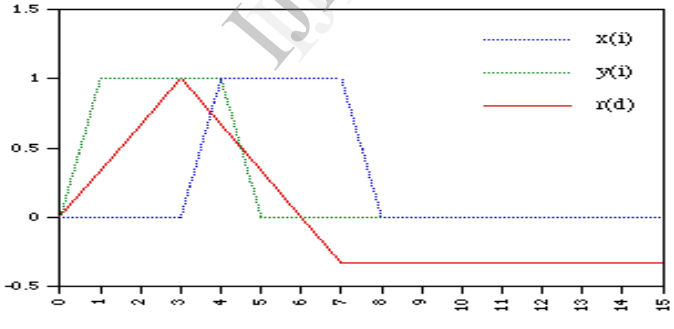

Figure 3: Two rectangular pulses

The maximum correlation is achieved at a delay of 3. Considering the equations above, what is happening is the second series is being slid past the first, at each shift the sum of the product of the newly lined up terms in the series is computed. This sum will be large when the shift (delay) is such that similar structure lines up. This is essentially the same as the so called convolution except for the normalization terms in the denominator.

3.2 AUTO CORRELATION:

When the correlation is calculated between a series and a lagged version of itself it is called autocorrelation. A high correlation is likely to indicate a periodicity in the signal of the corresponding time duration. The correlation coefficient at lag k of a series x_0, x_1, x_2 ...x_{N-1} is normally given as

$$autocorr(k) = \frac{\sum_{i=0}^{N-1}(x_i - mx)(x_{i+k} - mx)}{\sum_{i=0}^{N-1}(x_i - mx)^2} \quad (9)$$

Where mx is the mean of the series, when the term i+k extends past the length of the series N two options are available. The series can either be considered to be 0 or in the usual Fourier approach the series is assumed to wrap, in this case the index into the series is (i+k) mod N.

If the correlation coefficient is calculated for all lags k=0, 1, 2...N-1 the resulting series is called the autocorrelation series or the correlogram. The autocorrelation series can be computed directly as above or from the Fourier transform as

$$fourier[autocorr(k)] = \left| fourier[x(i)]^2 \right| \quad (10)$$

That is, one can compute the autocorrelation series by transforming the series into the frequency domain, taking the modulus of each spectral coefficient, and then performing the inverse transform. Note that depending on the normalization used with the particular FFT algorithm, it has to scale by N.

This method for computing the auto correlation series is particularly useful for long series where the efficiency of the Fast Fourier Transform can significantly reduce the time required to compute the autocorrelation series.

Note that this is a special case of the expression for calculating the cross correlation using Fourier transforms. The Fourier transform of the cross correlation function is the product of the Fourier transform of the first series and the complex conjugate of the Fourier transform of the second series.

3.3 2D PATTERN IDENTIFICATION USING CROSS CORRELATION:

One approach to identifying a pattern within an image uses cross correlation of the image with a suitable mask. Where the mask and the pattern being sought are similar the cross correlation will be high. The mask is itself an image which needs to have the same functional appearance as the pattern to be found.

Consider Figure (4) where the image is shown in black and mask is shown in red. The mask is centered at every pixel in the image and the cross correlation calculated, this forms a 2D array of correlation coefficients.

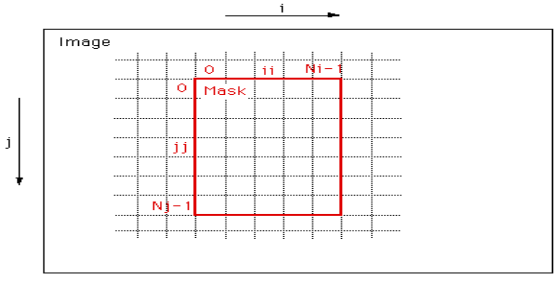

Figure 4: The image and mask for 2D Pattern Identification using Cross correlation.

The form of the un-normalized correlation coefficient at position (i, j) on the image is given by

$$r[i][j] = \sum_{jj=\frac{-Nj}{2}}^{jj<\frac{-Nj}{2}} \sum_{ii=\frac{-Ni}{2}}^{ii<\frac{-Ni}{2}} (mask[ii+\frac{Ni}{2}][jj+\frac{Nj}{2}] - \overline{mask})(image[i+ii][j+jj] - \overline{image}) \qquad (11)$$

Where $\overline{mask}$ is the mean of the masks pixels and $\overline{image}$ is the mean of the image pixels under (covered by) the mask.

The peaks in this cross correlation "surface" are the positions of the best matches in the image of the mask.

Issues

- The process can be extremely time consuming, the 2D cross correlation function needs to be computed for every point in the image. Calculation of the cross correlation function is itself a N^2 operation. Ideally the mask should be chosen as small as practicable.
- In many image identification processes the mask may need to be rotated and/or scaled at each position.
- This process is very similar to 2D filtering except in that case the image is replaced by an appropriately scaled version of the correlation surface.

3.4 PEAK SIGNALS-TO-NOISE RATIO:

An objective measure for the quality of a de-noised image would be very useful. One traditional measure for the closeness of two data sets is the Root Mean Squared Error, or RMSE. When ground truth is available, the two data sets could be the de-noised image f´(x,y) and the original image, f(x,y) Equation (12) calculates the RMSE in this case.

$$RMSE = \sqrt{\frac{1}{XY}\sum_{y=0}^{Y-1}\sum_{x=0}^{X-1}[f'(x,y) - f(x,y)]^2} \qquad (12)$$

The RMSE is proportional to the disparity between two images. In the case of two equivalent images, it is zero. For the case of additive zero-mean Gaussian noise, the RMSE between the noisy and original images is exactly equal to the noise standard deviation. The Peak Signal to Noise Ratio, or PSNR, is derived from the RMSE, and is measured in decibels (dB). This logarithmic measure is computed using Equation (13), where Z-1 is the maximum possible pixel intensity.

$$PSNR = 20\log_{10}\left(\frac{Z-1}{RMSE}\right)dB \qquad (13)$$

3.5 MEAN ABSOLUTE ERROR:

RMSE and PSNR use the square of the pixel difference. This penalizes large errors very heavily. For example, a single pixel in error by 100 will have the same contribution as 10,000 pixels in error by 1. An alternative measure, which aims to alleviate this potential problem, is the Mean Absolute Error, or MAE, calculated using Equation (14). The MAE penalizes errors by their magnitude, and is less likely, compared to RMSE, to be biased by occasional large errors.

$$MAE = \frac{1}{XY}\sum_{y=0}^{Y-1}\sum_{x=0}^{X-1}\left|f'(x,y) - f(x,y)\right| \qquad (14)$$

4. METHODOLOGY AND IMPLEMENTATION:

The program was developed in MATLAB in Windows system. The standard functions of MATLAB and MATLAB Image Processing Toolbox are used. Because of large amount of data processed, computers with at least 1GB of RAM are required. Speed of the processor is not crucial.

4.1 METHODOLOGY:

The methodology to compute Correlation coefficient, PSNR and MAE is explained as follows:

Step1: Collecting the DICOM images.
Step2: Convert the DICOM into binary image by apply thresholding to image.
Step3: Develop gradient images using appropriate edge detection function.
Step4: Mark the Foreground Objects using morphological operation.
Step6: Compute Background Markers.
Step7: Compute the Watershed Transform of the Segmentation Function.
Step8: Extraction of lung region.
Step9: Extraction of nodule by applying the region growing techniques.
Step10: Compute the correlation coefficient, PSNR and MAE between ROI without considering the noise and ROI by considering the noise.

4.2 IMPLEMENTATION:

In this section work done for processing lung image segmentation is explained. First by applying the watershed segmentation on the medical image the results are not properly segmented that is over segmentation occurs, now marking the fore ground and background objects using markers and applying watershed segmentation the desired results are realized. Implementation of the methodology explained in section 4.1 is explained as follows:

1. Input the noise added Digital Image:

The noise added DICOM is given as input to the proposed system.

2. Image preprocessing:

A typical DICOM image is converted as gray image for easy segmentation of unwanted portions of lung, and median filter is used to filter the noise.

3. Generate Segmentation Function:

One common application of watershed segmentation is to extract regions or blob-like objects of uniform or near-uniform intensity. Since a region with low intensity variation has small gradient, therefore in practice watershed segmentation often applies on gradient images instead of original images. In such cases, high gradient magnitudes are at object or region boundaries, while low gradient magnitudes occur inside regions or objects. The goal of this step is to generate gradient magnitude images that are to be used for later segmentation step. For example to this end, two Sobel filters, one is horizontal (Formula (15)) and the other is vertical (formula (16)), are applied on the cleaned image I from preprocessing step, respectively. The process generates two edge images, G_x and G_y. These images are then used to calculate gradient image G.

$$G_x = \begin{bmatrix} -1 & 0 & 1 \\ -2 & 0 & 2 \\ -1 & 0 & 1 \end{bmatrix} * I \qquad (15)$$

$$G_y = \begin{bmatrix} -1 & -2 & -1 \\ 0 & 0 & 0 \\ 1 & 2 & 1 \end{bmatrix} * I \quad (16)$$

$$G = \sqrt{G_x^2 + G_y^2} \quad (17)$$

4. Locate foreground markers:

One reason that leads to over-segmentation results from a large number of potential but trivial regional minima. The goal of this step is to locate regional minima that are more likely containing nodules.

A regional minima has to satisfy three conditions

1) Surrounded by higher value;
2) Region areas are bigger than a predefined threshold value; and
3) Points inside a region are connected and are of the same intensity value.

In proposed approach, since markers are picked from original images and nodules have higher intensity values than its surroundings, the foreground markers are located at regional maxima. The locations of these regional maxima are mapped back for segmentation on gradient images on last step. To pick foreground markers, a variety of morphological functions are applied: opening by reconstruction, closing by reconstruction. Opening by reconstruction is erosion followed by image morphological reconstruction. This operation is used to remove some of the bright pixels from the edges of regions. Depending on the size of the structure element, the step will also effectively remove some regional maxima. Closing-by-reconstruction is a dilation followed by image reconstruction. This operation is applied to shrink background color holes inside regions. This will actually lead to the merging of regions, which also remove trivial regional maxima. Compared with normal opening and closing, opening by reconstruction and closing by reconstruction are less destructive and can maintain an object's shape better. At last, regional maxima are selected using 4 or 8-neighborhood. Pixels inside are connected with same intensity value for example't', whose external boundary pixels all have value less than *t*.

5. Compute Background markers:

While the foreground markers determines allowable regions to start the flooding process, the background markers constrain the flooding process so that it will stop at the edges of the objects we are trying to segment. To this end, an adaptive thresholding segmentation method is applied on the original image. After that, with holes inside regions filled and very small regions removed, the segment boundaries are used as background markers in our approach. After this step produce the image with both foreground and background markers overlaid on it.

6. Watershed Segmentation:

In this step, first the locations of foreground makers and background markers are mapped to the gradient magnitude image. And then modify the gradient magnitude image so that its only regional minima occur at those locations where foreground and background markers are. Finally, watershed segmentation is performed on the modified gradient magnitude image. And region growing techniques are employed to extract the nodules.

7. Adding Noise: The above procedure is repeated by considering various noises such as Gaussian, Poisson, Salt & Pepper and speckle noises and by different gradient operators like Average, Gaussian, Laplacian, Sobel, Prewitt, Log and Unsharp.

8. Correlation coefficient, PSNR and MAE:

Evaluated the performance and tabulated the result by computing the correlation coefficient, peak signal to noise ratio and mean absolute error for the nd the ROI obtained in step3, and ROI obtained in the step 4 for various gradient operators in presence of different noises.

9. Local variations of the image can change dramatically the results. This effect is worsened by the use of high pass filters to estimate the gradient, based on the correlation coefficient and PSNR best filter is identified for estimating the gradient.

5. RESULTS:

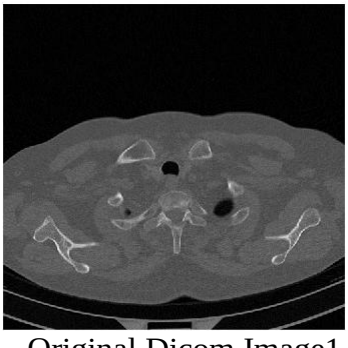
Original Dicom Image1


Original ROI Image2

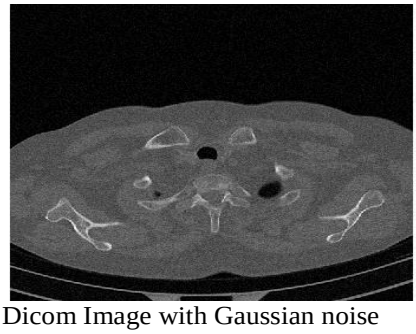
Dicom Image with Gaussian noise

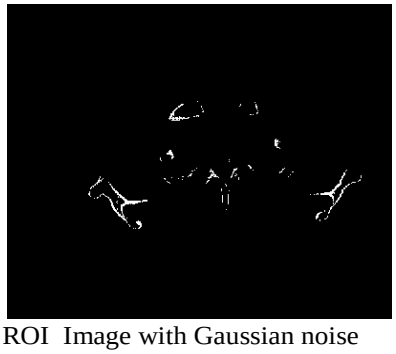
ROI Image with Gaussian noise

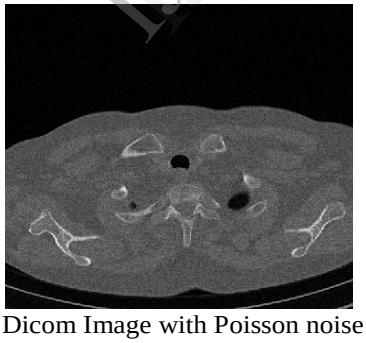
Dicom Image with Poisson noise

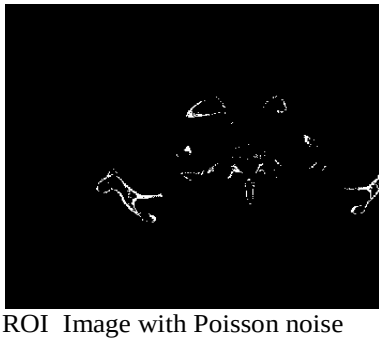
ROI Image with Poisson noise

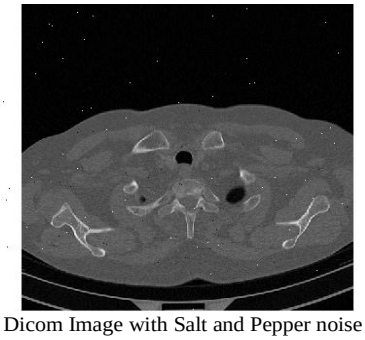
Dicom Image with Salt and Pepper noise

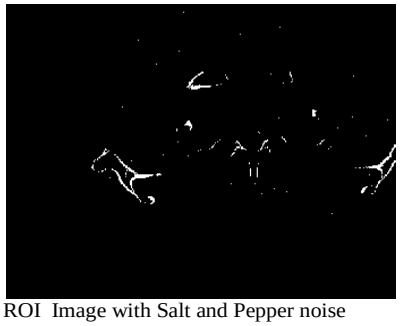
ROI Image with Salt and Pepper noise

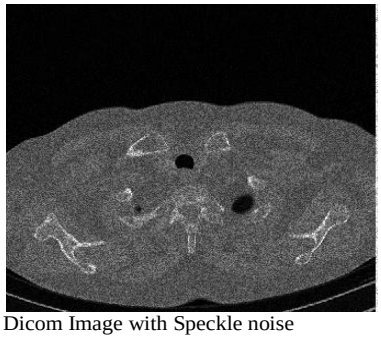
Dicom Image with Speckle noise

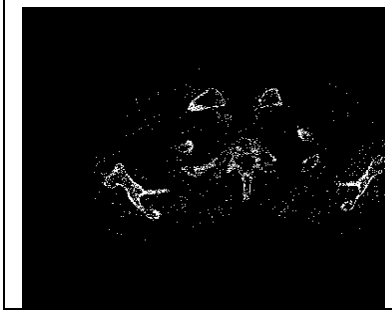

ROI Image with Speckle noise

Figure 5: original Dicom and ROI segmentation with Gaussian, poission, salt and pepper and speckle noise for image 1.

Figure (5) represents Dicom image and ROI segmentation for image (1) by adding Gaussian, poission, salt and pepper and speckle noise. Tables (2), (3) & (4) represent Correlation coefficient, Peak Signal to Noise Ratio and Mean Absolute Error between Region of interest with and without noise for image 1.

Table 2: Correlation coefficient between Region of interest with and without noise for image 1.

Operator / Noise	Average	Gaussian	Laplacian	Sobel	Prewitt	Log	Unsharp
Gaussian	0.8846	**0.8825**	0.8845	0.8835	0.8898	0.8866	0.8829
Poisson	0.8175	0.8172	0.8194	**0.8217**	0.8217	0.8159	0.8244
Salt&pepper	0.9828	0.9830	0.9825	**0.9836**	0.9816	0.9806	0.9827
Speckle	0.4667	0.4771	0.4799	0.4701	**0.4805**	0.4786	0.4737

Table 3: Peak Signal to Noise Ratio between Region of interest with and without noise for image 1.

Operator / Noise	Average	Gaussian	Laplacian	Sobel	Prewitt	Log	Unsharp
Gaussian	77.8893	77.7791	77.9300	77.869	78.118	78.0547	77.7890
Poisson	75.6425	75.6850	75.6606	75.758	75.691	75.6243	75.7714
Salt&pepper	86.3504	86.4222	86.2798	86.569	86.074	85.8152	86.3504
Speckle	68.5452	68.7174	68.7531	68.662	68.790	68.7284	68.7630

Table 4: Mean Absolute Error between Region of interest with and without noise for image 1.

Operator / Noise	Average	Gaussian	Laplacian	Sobel	Prewitt	Log	Unsharp
Gaussian	0.0011	0.0011	0.0010	0.0011	0.0010	0.0010	0.0011
Poisson	0.0018	0.0018	0.0018	0.0017	0.0018	0.0018	0.0017
Salt&pepper	0.0002	0.0001	0.0002	0.0001	0.0002	0.0002	0.0002
Speckle	0.0091	0.0087	0.0087	0.0088	0.0086	0.0087	0.0086

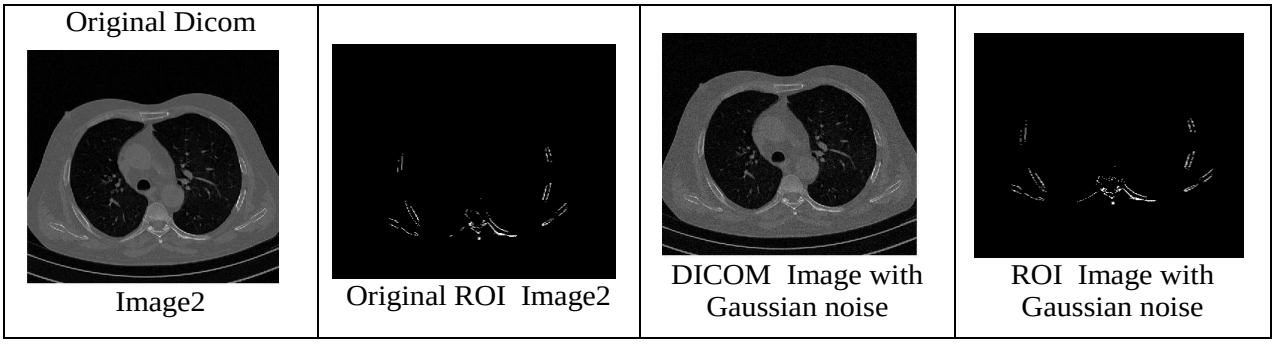

Figure 6: original Dicom and ROI segmentation with Gaussian noise for image 2.

Figure (6) represents Dicom image and ROI segmentation for image (1) by adding Gaussian, poission, salt and pepper and speckle noise. Tables (5), (6) & (7) represent Correlation coefficient, Peak Signal to Noise Ratio and Mean Absolute Error between Region of interest with and without noise for image 1.

Table . 5: Correlation coefficient between Region of interest with and without noise for image 2.

Operator / **Noise**	**Average**	**Gaussian**	**Laplacian**	**Sobel**	**Prewitt**	**Log**	**Unsharp**
Gaussian	0.8842	0.8877	0.8711	0.8867	0.8509	0.8867	0.8591
for image	0.7931	0.7902	0.7971	0.7944	0.8200	0.7940	0.7959
Salt&pepper	0.9740	0.9729	0.9732	0.9764	0.9816	0.9748	0.9776
Speckle	0.3986	0.4021	0.3958	0.3822	0.3895	0.3979	0.4009

Table 6: Peak Signal to Noise Ratio between Region of interest with and without noise for image 2.

Operator / **Noise**	**Average**	**Gaussian**	**Laplacian**	**Sobel**	**Prewitt**	**Log**	**Unsharp**
Gaussian	79.6858	79.7321	79.2483	79.763	79.440	79.716	79.6407
Poisson	76.5470	76.5694	76.7374	76.524	77.436	76.607	76.7063
Salt&pepper	86.2103	86.0083	86.0746	86.645	87.769	86.350	86.8798
Speckle	68.3672	68.3333	68.2103	68.324	68.208	68.306	68.2598

Table 7: Mean Absolute Error between Region of interest with and without noise for image 2.

Operator / **Noise**	**Average**	**Gaussian**	**Laplacian**	**Sobel**	**Prewitt**	**Log**	**Unsharp**
Gaussian	0.0007	0.0007	0.0008	0.0007	0.0009	0.0007	0.0009
Poisson	0.0014	0.0014	0.0014	0.0014	0.0012	0.0014	0.0014
Salt&pepper	0.0002	0.0002	0.0002	0.0001	0.0001	0.0002	0.0001
Speckle	0.0095	0.0095	0.0098	0.0096	0.0098	0.0096	0.0097

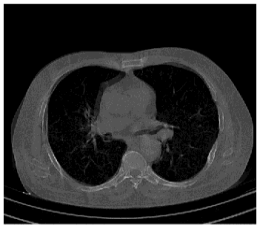

Original Dicom Image3

Original ROI

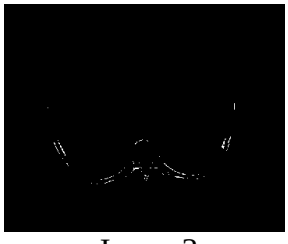

Image3

DICOM Image with Gaussian noise

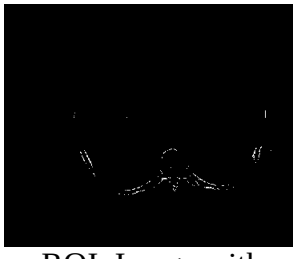

ROI Image with Gaussian noise

Figure 7: original Dicom and ROI segmentation with Gaussian noise for image 3.

Figure (7) represents Dicom image and ROI segmentation for image (1) by adding Gaussian, poission, salt and pepper and speckle noise. Tables (8), (9) & (10) represent Correlation coefficient, Peak Signal to Noise Ratio and Mean Absolute Error between Region of interest with and without noise for image 3.

Table 8: Correlation coefficient between Region of interest with and without noise for image 3.

Operator / Noise	Average	Gaussian	Laplacian	Sobel	Prewitt	Log	Unsharp
Gaussian	0.8499	0.8543	0.8380	0.8467	0.8359	0.8359	0.8290
Poisson	0.7527	0.7609	0.7259	0.7331	0.7509	0.7591	0.7574
Salt&pepper	0.9745	0.9610	0.9661	0.9624	0.9631	0.9684	0.9631
Speckle	0.3228	0.3449	0.3422	0.3210	0.3396	0.3395	0.3423

Table 9: Peak Signal to Noise Ratio between Region of interest with and without noise for image 3.

Operator / Noise	Average	Gaussian	Laplacian	Sobel	Prewitt	Log	Unsharp
Gaussian	81.3481	81.5086	80.9609	81.237	80.819	80.819	80.7402
Poisson	78.5927	78.6892	78.2708	78.304	78.677	78.876	78.6649
Salt&pepper	89.1522	87.2140	87.8690	87.391	87.482	88.183	87.4827
Speckle	69.8997	70.2000	70.0157	70.881	70.194	70.340	69.9844

Table 10: Mean Absolute Error between Region of interest with and without noise for image 3.

Operator / Noise	Average	Gaussian	Laplacian	Sobel	Prewitt	Log	Unsharp
Gaussian	0.0005	0.0005	0.0005	0.0005	0.0005	0.0005	0.0005
Poisson	0.0009	0.0009	0.0010	0.0010	0.0009	0.0008	0.0009
Salt&pepper	0.0001	0.0001	0.0001	0.0001	0.0001	0.0001	0.0001
Speckle	0.0067	0.0062	0.0065	0.0053	0.0062	0.0060	0.0065

6. CONCLUSION:

Nodule detection is one of the major problems in medicine and the researches are going on till now to improve the performance of present equipments. This is because survival rate should be increased if cancer is detected in early stages. A program was implemented to extract ROI, i.e. lung region that consists of blood vessels and nodules from the major lung portion. It is based on mainly segmentation and applying watershed transform and then morphological operations to extract the region of interest. The validity of the results was

performed by applying the procedure on DICOM image in different noises. The detailed view of nodules and blood vessels was observed in each angle. This makes easy way to detect and study the ROI. This method can be used as an initial step for Computer Aided Diagnosis.

From visual examination of the results considering Correlation coefficient, Peak Signal to Noise Ratio (PSNR) and Mean Absolute Error (MAE) it can be noticed that:

- Laplacian operator performs better and unsharp operator performs poor in Gaussian noise environment.
- In Poisson noise environment, Gaussian operator exhibits better performance and Laplacian exhibits poor performance.
- In Salt & Pepper noise conditions Gaussian operator exhibits superior performance and Prewitt exhibits inferior performance.
- Sobel operator exhibits superior performance, and Gaussian operator inferior in Speckle noise environment.

7. REFERENCES:

1) Krishnan Nalla perumal, K. Krishna veni, Justin Varghese, S. Saudia , S. Annam, P. Kumar." A novel Multi-scale Morphological Watershed Segmentation Algorithm" in International Journal of Imaging Science and Engineering (IJISE).
2) Bram van Ginneken*, Bart M. ter Haar Romeny, and Max A. Viergever, Member IEEE," Computer-Aided Diagnosis in Chest Radiography:A Survey", IEEE transactions on medical imaging, vol.20,no.12, December 2001.
3) Anitha. S1 and Sridhar.S2." segmentation of lung lobes and nodules in CT images", Signal & Image Processing : An International Journal(SIPIJ) Vol.1, No.1, September 2010.
4) Ning Xu*a*, Narendra Ahuja*a* and Ravi Bansal*b,"* Automated Lung Nodule Segmentation Using Dynamic Programming and EM Based Classification"**,** ECE Department and Beckman Institute, University of Illinois at Urbana-Champaign, IL 61801*b*Siemens Corporate Research, Inc. Princeton, NJ 08540.
5) Zhao Yu-qian1, 2, Gui Wei-hua2, Chen Zhen-cheng1, Tang Jing-tian1, Li Ling-yun1," Medical Images Edge Detection Based on Mathematical Morphology", Proceedings of the 2005 IEEE
6) Rafael C. Gonzalez & Richard E. Woods, Digital image processing- Addison Wesley/Pearson education, 3rd Edition, 2008.
7) O.s.pianykh - digital imaging and communications in medicine (DICOM) , a practical introduction and survival guide, ISBN 978-3-540-74570-9.
8) S. jayaraman, S. Esakkirajan, and T. Veerakumar, Digital Image Processing, Tata McGraw Hill, 2009,368-408.
9) Sangram Bana, Nirbhay Ahlawat, and Dr. Davinder kaur, " Image Segmentation Schemes Applied to Microscopic Images using MATLAB. ", International Journal of Advanced Engineering sciences and Technologies, Vol. No.9, Issue No.1, pp.146-158.